Thermal 3D Modeling and Analysis of PMSMs with Inter-Turn Faults

Felix Hoffmann, Simon Foitzik, Martin Doppelbauer
Institute of Electrical Engineering (ETI)
Karlsruhe Institute of Technology (KIT)
Kaiserstr. 12, 76131 Karlsruhe, Germany
felix.hoffmann@kit.edu

***Abstract*—Intern-turn faults are one of the most common causes of machine failure. The propagation of this fault is mainly determined by the local fault temperature. In this paper, we present a 3D analytical approach to determine the temperature distribution inside the windings during an inter-turn fault. To do so, a coupled electromagnetic-thermal model is used. The fault loss is calculated in the electromagnetic model and serves as an input for the thermal model. The thermal model consists of an extended layer approach, which we adapted to simulate inter-turn faults. It can be seen that the fault's location and the fault area have a major influence on the maximum temperature rise. For a fault in the active region close to the stator yoke the maximum temperature rises for a fault loss of $10\,\mathrm{W}$ by $8.8\,\mathrm{K}$, whereas the maximum temperature rises by $137.6\,\mathrm{K}$ in the middle of the end winding. The maximum temperature rise is highly dependent on the fault's location and the maximum temperature rise increases, the closer to the air gap the fault occurs. The closer it is in axial direction to the middle of the end windings, the larger the maximum temperature rise.**

***Index Terms*—inter-turn fault, thermal modeling, fault modeling, lumped-circuit analysis, permanent magnet synchronous machines**

I. Introduction

The lifetime and reliability of electrical machines is besides the bearings, mainly limited by stator winding faults [1]. In drive systems with Voltage Source Inverters (VSIs), inter-turn faults are often the origin of more severe faults, such as phase-to-phase or phase-to-ground faults and result from constant thermal, electrical, mechanical and environmental stresses [2]. Therefore, the propagation of an inter-turn fault can lead to a complete drive system failure, which must be prevented especially in safety critical applications like all-electric aircraft. The propagation of an inter-turn fault is mainly determined by the temperature locally at the fault [3]. A temperature rise at the fault location is caused by the generated heat P_{fault} of the inter-turn fault. In general there exist multiple approaches of analyzing the thermal behavior of an electrical machine [4]-[10]. Except [9], where they use a partial Finite Element Analysis (FEA) model, the authors are focusing on analytical lumped circuit models and validated them with FEA approaches or experimental results. Modeling thermal inter-turn faults require not only a fast computational time, but also a high local accuracy as the thermal behavior of an electrical machine in case of a failure is a local phenomenon. There already exist several approaches to analyze the thermal behavior of electrical machines with inter-turn faults. These approaches can be separated on the one hand into FEA and analytical approaches. On the other hand, they can be separated into 2D and 3D approaches. In [11], the authors present a 2D analytical model and in [12], the authors present a 2D-FEA model. Both models neglect the temperature distribution in axial direction, which is very crucial. Further, the total mass of a wire is concentrated in one point, which makes it impossible to simulate the local phenomenon of an inter-turn fault. In [13], the authors present a 3D-FEA model and consequently compensate this drawback. Nevertheless, the calculation of this model is very time consuming and a detailed single wire 3D computer-aided design (CAD) model is necessary.

In this paper, we present a novel 3D analytical approach to analyze the thermal behavior of electrical machines with inter-turn faults. In [14], we presented an extended layer approach to thermally model the stator slot of electrical machines. Now, we extend the existing 2D model to a 3D model, with the possibility to place inter-turn-faults within the stator winding. This modeling approach combines the advantages of a fast computational time and also considers the propagation of the fault in axial direction. In addition, the approach has a higher resolution close to the fault, which increases the accuracy of the model. The input for the thermal model is provided by an electromagnetic fault model, which we presented in [15].

II. Modeling

The modeling is divided into the electromagnetic and thermal domain. The electromagnetic model determines the different heat sources and forwards them to the thermal model. The thermal and electromagnetic model are both set up in MATLAB® Simscape™.

A. Electromagnetic Modeling

The analytical model for the simulation of Permanent Magnet Synchronous Machines (PMSMs) with stator winding faults describes the electromagnetic behavior on turn level and is validated with FEA simulations [15]. Both models show good accordance and the computational time of the analytical model is about 200 times faster compared to the FEA model. This is important for coupling the two domains, because the thermal time constant is much larger than the electromagnetic one. Fig. 1 shows the phase arrangement of the analyzed machine and an exemplary inter-turn fault in phase Ph1. The stator winding is separated in a faulty and healthy part, which allows the simulation of various inter-turn, phase-to-phase or phase-to-ground faults. The corresponding upper half of the cross section is shown in Fig. 2. The colors of the slots match with the colors of the phase arrangement. In general, an inter-turn fault causes a circulating current I_{F} in the shorted turns. This fault current depends on the operating point and the fault combination, which is given by the number of shorted turns w_{F}

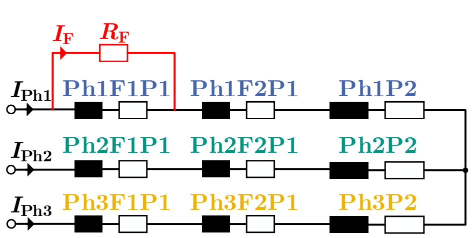

Fig. 1. Phase arrangement of the stator winding with an inter-turn fault

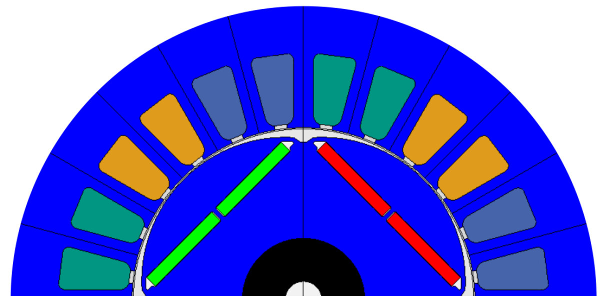

Fig. 2. Upper half of the cross section of the analyzed PMSM

and the fault resistance R_{F}. The fault combination cannot be determined during operation, since there are multiple solutions [16]. The power loss generated by the fault is calculated by:

$$P_{\text{fault}} = I_{\mathrm{F}}^2 \cdot R_{\mathrm{F}} \tag{1}$$

An inter-turn fault causes second harmonics in the dq-voltages, due to the arising asymmetry in the stator winding. These amplitudes can be used to estimate the severity of the fault and the power loss can be reduced by an adapted operating point [17]. At constant electrical power of the machine, the circulating fault current also causes a reduction of the average torque.

B. Thermal Modeling

In [14], we present a thermal model of a stator slot in electrical machines. The main idea is to separate the slot into a predefined number of layers, as the temperature distributes in layers for round windings. The predefined number of layers is chosen to be six to reach a high accuracy and keeping the computational effort low at the same time. A detailed analysis for this selection was done in [14] and is not further explained in this paper. All layers itself are separated into a copper layer, where the losses are injected, and two layers of resin and insulation lacquer, as shown in Fig. 3. With a separation in all four directions, hot spots can be determined besides the average winding temperature.

In [18], we extended this approach in axial direction to model a tooth-coil winding in electrical machines including radial and axial heat flux. To do so, the stator coil is discretized along the wire's length and multiple segments are connected in axial direction, which is displayed in Fig. 4. Every segment represents a cross section of the coil, as shown in Fig. 3. The coordinate system is rotating and always in line with the wire's

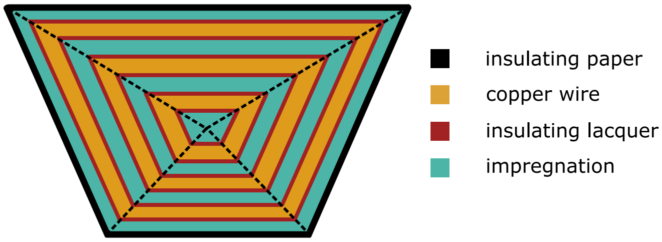

Fig. 3. Layer arrangement in a segment (2D)

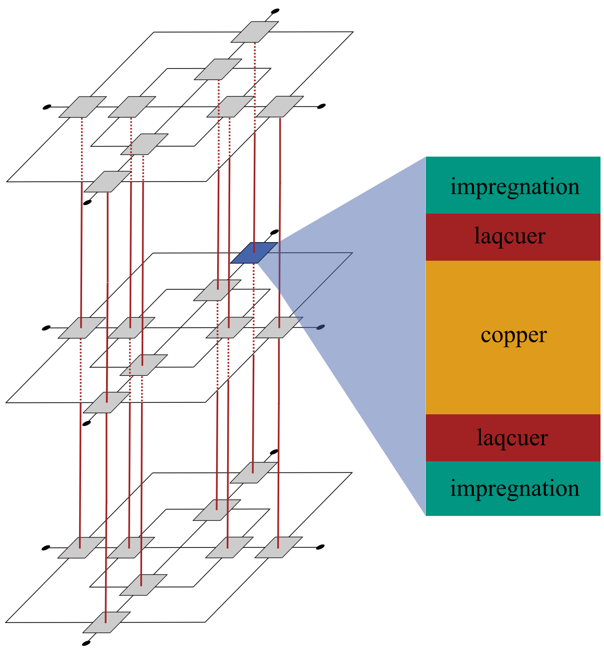

Fig. 4. Axial connection of segments (3D) for a quarter stator coil

direction. Using this approach, the geometry and heat flux can always be described in radial and axial direction to the wires and no complex transformation in the cartesian coordinate system is needed. It was shown that a good trade-off between accuracy and simulation time was reached with a discretization of two segments inside the slot and four segments inside the end windings for a quarter of the stator coil. A detailed analysis can be found in [18]. However, it was shown that the difference compared to two segments in the end windings is comparable small and decreases the computational time. In the following, two segments in the slot and two segments in the end windings are used. The described model is independent of the wire arrangement and is therefore also valid for a distributed winding.

For a thermal fault model, it is essential to model a whole stator coil, as the temperature distribution is not symmetric

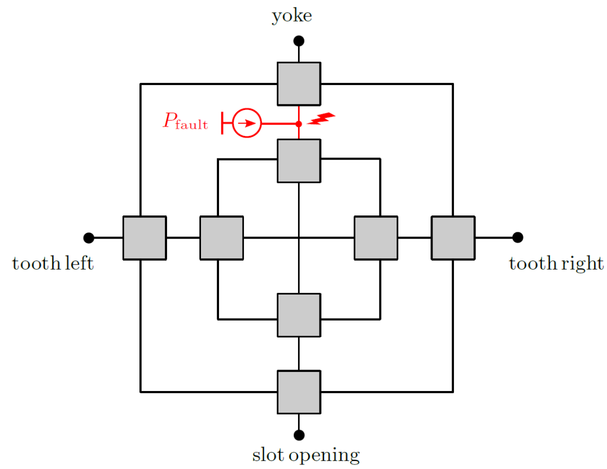

Fig. 5. Graphical representation of the thermal fault model in a segment (2D)

anymore. The heat flux to neighboring stator slots and stator coils is neglected due to the local fault phenomenon. To model an inter-turn fault, two layers inside one segment are shorted. This is equivalent to a physical copper contact between two wires. Fig. 5 shows an exemplary fault modeling inside a segment. Since the temperature rise caused by the local power loss is a local phenomenon, the thermal mass of the shorted layers is important. To get a better modeling of the local phenomenon in axial direction, the fault segment itself is split up into three different segments. The middle segment describes the fault segment, which can be seen in Fig. 5, and its height is chosen to a predefined value depending on the fault layer to determine a fault area. This fault area can be interpreted as the physical contact area of the copper of the shorted wires. The other two segments are used to get the same thickness of the remaining segments. Fig. 6 shows the separation of the fault segment in axial direction and their integration in the full model. For the sake of simplicity, just a quarter of the whole stator coil is shown, whereas the model considers the whole stator coil. This means that the model has a higher resolution in the fault region and models a physical realistic fault area. Shorting two layers inside one segment with full height would lead to a drastic overestimation of the fault area and would have a major effect on the maximum temperature rise as explained later on. The fault loss P_{fault} calculated by the electromagnetic model is directly forwarded to the fault location.

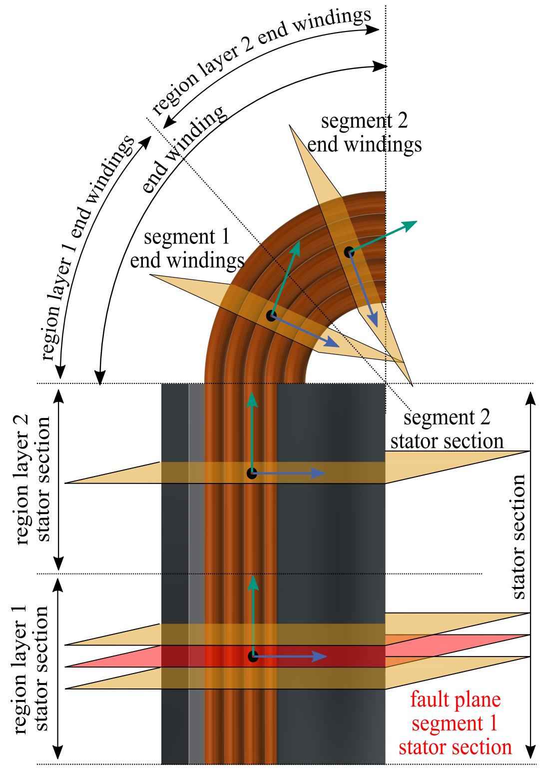

Fig. 6. Graphical representation of the thermal fault model in a quarter of a coil (3D)

III. Machine Under Test

The used machine is an interior PMSM with 4 poles and 24 slots. The maximum output power of the machine is $12\,\mathrm{kW}$ with a maximum rotational speed of $8000\,\mathrm{min}^{-1}$. Every slot is filled with 43 windings with a copper diameter of $1\,\mathrm{mm}$ and a insulation lacquer thickness of $0.04\,\mathrm{mm}$. The machine has a trickle impregnation with a thermal conductivity of $0.2\,\mathrm{W\,m^{-1}\,K^{-1}}$ and it is assumed that no residual air gaps are in between the wires or inside the stator slot. The machine has a water cooling jacket with an assumed cooling temperature of $65\,°\mathrm{C}$.

IV. Results

Under healthy conditions, the machine is always simulated at a reference loss point with copper losses of $P_{\mathrm{cu}} = 750\,\mathrm{W}$ and iron losses of $P_{\mathrm{fe}} = 100\,\mathrm{W}$. This operation point represents a point of continuous power operation. We do not further focus on the fault combination in this paper, since various combinations of the operation point, the fault resistance R_{F} and the number of shorted turns w_{F} lead to the same power loss, as indicated in Eq. (1). For the first simulation an intern-

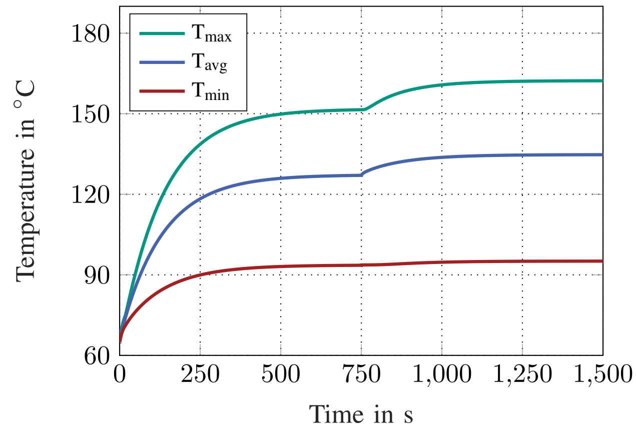

Fig. 7. Maximum, average and minimum winding temperature for a fault in the middle of the active region close to the stator yoke at $t = 750\,\mathrm{s}$, a fault loss of $P_{\mathrm{fault}} = 10\,\mathrm{W}$ and a fault area of $A_{\mathrm{fault}} = 1\,\mathrm{mm}^2$

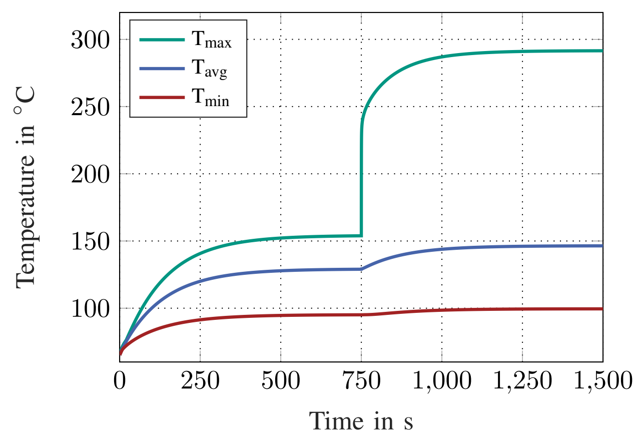

Fig. 8. Maximum, average and minimum winding temperature for a fault in the middle of the end windings at $t = 750\,\mathrm{s}$, a fault loss of $P_{\mathrm{fault}} = 10\,\mathrm{W}$ and a fault area of $A_{\mathrm{fault}} = 1\,\mathrm{mm}^2$

turn fault occurs at $t = 750\,\mathrm{s}$ with a power loss of $10\,\mathrm{W}$ and a fault area of $1\,\mathrm{mm}^2$. Two scenarios are analyzed in this case. Fig. 7 shows a fault in the middle of the active region close to the stator yoke, which corresponds to the location of the coolest winding temperature and can be handled as a best case scenario. On the other hand, Fig. 8 depicts a fault in the middle of the end windings, which corresponds to the hottest point in the windings and can be handled as a worst case scenario. It should be noted that the overall maximum, average and minimum winding temperatures are analyzed and therefore these temperatures need to be the same for different fault scenarios in healthy condition before the fault occurs. The effect on different fault scenarios on the overall winding temperatures is analyzed afterwards. For the best case scenario, the maximum and average temperatures rise by 8.8 K and 7.7 K. Therefore, the maximum temperature rise is due to an overall temperature rise of the winding temperature, which results from an additional power loss. As the fault occurs in a relatively cold region, the maximum temperature rise is limited. On the other hand, the maximum and average temperature for the worst case scenario rise by 137.65 K and 17.4 K. The maximum temperature rise is significantly larger compared to the average temperature rise as the fault power is generated directly in the hottest point of the machine. This is even more severe for the temperature rise within the first second after the fault occurs, which is given by 80 K. In this case an instant counteraction is needed, to prevent a further temperature rise at the fault locally.

The temperature rise due to the fault is highly dependent on the location of the fault. Therefore, a detailed analysis is needed, to characterize the impact of the fault depending on the fault's location. To do so, the fault is analyzed in one segment. The fault's location is varied in radial direction. Fig. 9 shows the maximum, average and minimum steady-state winding temperatures for a fault in the first segment and a varying layer in radial direction for a fault loss of $P_{\mathrm{fault}} = 10\,\mathrm{W}$ and a fault area of $A_{\mathrm{fault}} = 1\,\mathrm{mm}^2$. The segment corresponds to the axial middle location of the slot. The layers in lower radial direction correspond to the location from the middle of the slot to the air gap, where the fault between layer 1 and 2 represents a fault in the middle of the slot and a fault between layer 5 and 6 a fault close to the air gap. It can be seen that the fault's location in radial direction for a fault in the axial center of the active region has almost no influence on the minimum and average temperature. The maximum steady-state winding temperature is highly dependent on the fault layer and is decreasing in an exponential shape from a fault in the middle of the slot to a fault close to the air gap. The maximum temperature is decreasing from 219.4 °C down to 163.3 °C. The further out the fault occurs in radial direction, the shorter is the thermal path to the cooling medium and therefore the maximum temperature is decreasing. The average and minimum temperatures do not rise depending on the fault's location as the fault occurs in the middle of the active region, which has a short thermal path to the cooling medium. Since the fault power is for all fault's location the same, also the same temperature rise in the minimum and average temperatures is visible.

The other main factor to characterize the impact of the fault's location is the location in axial direction. Fig. 10 shows the maximum, average and minimum steady-state winding temperatures for a fault in the middle of the coil and a varying segment in axial for a fault loss of $P_{\mathrm{fault}} = 10\,\mathrm{W}$ and a fault area of $A_{\mathrm{fault}} = 1\,\mathrm{mm}^2$. Segment 1 represents a fault in the axial middle of the active region, whereas Segment 4

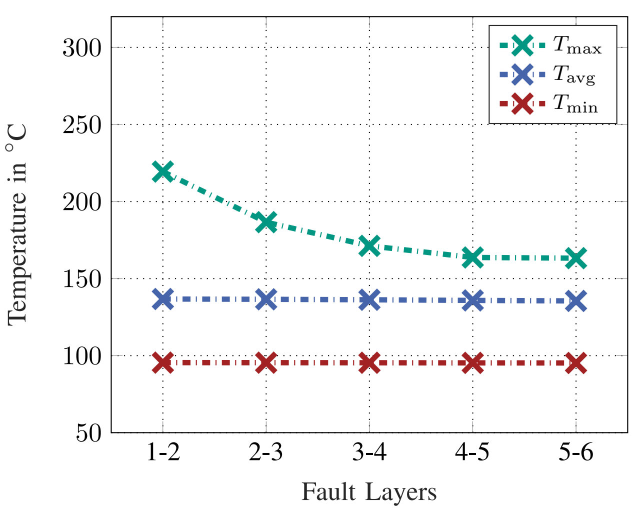

Fig. 9. Maximum, average and minimum steady-state winding temperatures for a fault in the axial center of the active region and a varying fault layer in radial direction at $t = 750\,\mathrm{s}$, a fault loss of $P_{\mathrm{fault}} = 10\,\mathrm{W}$ and a fault area of $A_{\mathrm{fault}} = 1\,\mathrm{mm}^2$

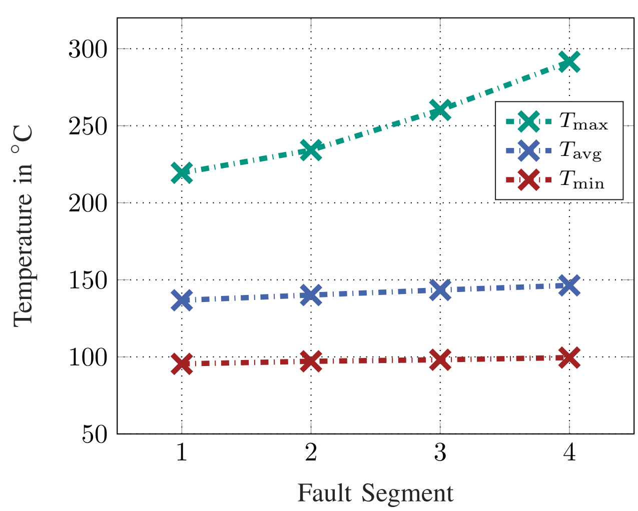

Fig. 10. Maximum, average and minimum steady-state winding temperatures for a fault in the middle of the and a varying fault segment in axial direction at $t = 750\,\mathrm{s}$, a fault loss of $P_{\mathrm{fault}} = 10\,\mathrm{W}$ and a fault area of $A_{\mathrm{fault}} = 1\,\mathrm{mm}^2$

represents a fault in the middle of the end windings. It is visible that the axial direction has a major influence on the maximum steady-state winding temperature. The maximum temperature is rising from $219.4\,°\mathrm{C}$ for a fault in the center of the axial region up to $291.5\,°\mathrm{C}$ for a fault in the middle of the end windings. On the other side, the minimum and average overall winding temperatures have a minor influence depending on the fault's location. The minimum temperature is rising from $95.5\,°\mathrm{C}$ to $99.5\,°\mathrm{C}$ and the average winding temperature is rising from $136.7\,°\mathrm{C}$ up to $146.4\,°\mathrm{C}$. This is due to the fact that the closer the fault is to the center of the end windings, the longer is the thermal path to the cooling medium as the heat is dissipated in axial winding direction through the active region to the cooling medium. Therefore, the same fault loss leads to a higher maximum winding temperature, the closer the fault is to center of the end windings. Compared to Fig. 9, a temperature rise in the average and minimum temperatures is also visible. Since the maximum temperature rise in the middle of the end windings is comparable large to the temperature rise in the slot, it will not just be a local effect of temperature rise. The significant local temperature rise will therefore have a influence on the overall average winding temperature. The same effect applies for the minimum winding temperature, whereas it is almost neglectable.

The last analyzed cruical parameter of modeling and characterizing an inter-turn fault is the fault area A_{fault}. This parameter describes the touching area of the two copper wires and has therefore a major influence on the heat transfer. Fig. 11 displays the effect of a changing fault loss P_{fault} from $0\,\mathrm{W}$ to $20\,\mathrm{W}$ and a varying fault area from $0.01\,\mathrm{mm}^2$ to $10\,\mathrm{mm}^2$ on the temperature rise of the maximum winding temperature. As the fault area A_{fault} is not known during the whole fault process, this is a qualitative analysis, how it will effect the maximum temperature rise inside the stator winding.

It can be seen that for fault areas below $0.1\,\mathrm{mm}^2$ the temperature rise is more than $196\,\mathrm{K}$ for a power loss of $10\,\mathrm{W}$. Such an increase in temperature would lead to a severe damage of the surrounding insulation. The larger the fault area gets, the lower the temperature rise is. This is clear as the thermal resistance is decreasing with an increasing fault area. For an increase of the power loss, the temperature rise is also increasing, as more heat is generated in the fault location. For a fault area of $2\,\mathrm{mm}^2$ the maximum winding temperature increases by $116.5\,\mathrm{K}$ for

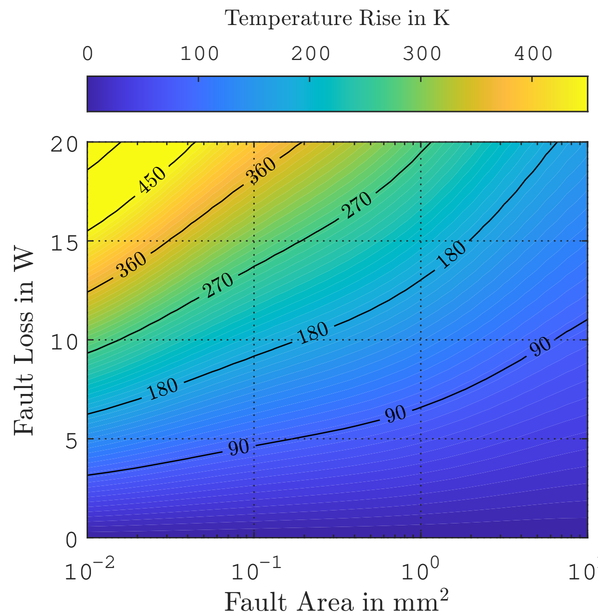

Fig. 11. Temperature rise of the maximum winding temperature in the middle of the end winding for a varying power loss from $0\,\mathrm{W}$ to $20\,\mathrm{W}$ and a varying fault area from $0.01\,\mathrm{mm}^2$ to $10\,\mathrm{mm}^2$

$10\,\mathrm{W}$. This means that for small fault areas the thermal stress is increased and significantly decreases for fault areas larger than $1\,\mathrm{mm}^2$. This positive effect indicates that the more energy is released due to the fault, the more the insulation gets damaged and the larger the fault area becomes.

V. Conclusion and Future Work

We presented a novel approach to analyze the temperature distribution inside a PMSM in case of an inter-turn fault using a 3D analytical approach. An extended layer approach is used, where a fault model is applied. The maximum temperature rise is besides the power loss highly dependent on the location of the fault and the area of the touching copper wires. It is shown that the closer a fault is to the center of the end windings, the larger is the maximum temperature rise, whereas it is almost not affected, if a fault in the center of the active region occurs. On the other hand, a fault in the center of the coil shows a severe impact on the maximum winding temperature compared to a fault at the radial outside of a coil. In our future work, we will use this thermal fault model to simulate transient fault scenarios, where a temperature dependent fault-tolerant control scheme is designed. The impact of this fault-tolerant control scheme on the temperature propagation in case of an inter-turn fault will be investigated.

REFERENCES

[1] Motor Reliability Working Group and others, "Report of large motor reliability survey of industrial and commercial installations, part i," *IEEE Trans. Industrial Applications*, vol. 1, no. 4, pp. 865–872, 1985.

[2] A. H. Bonnett and G. C. Soukup, "Cause and analysis of stator and rotor failures in three-phase squirrel-cage induction motors," *IEEE Transactions on Industry applications*, vol. 28, no. 4, pp. 921–937, 1992.

[3] M. A. Cash, T. G. Habetler, and G. B. Kliman, "Insulation failure prediction in ac machines using line-neutral voltages," *IEEE Transactions on Industry Applications*, vol. 34, no. 6, pp. 1234–1239, 1998.

[4] D. Staton, A. Boglietti, and A. Cavagnino, "Solving the more difficult aspects of electric motor thermal analysis in small and medium size industrial induction motors," *IEEE Transactions on Energy Conversion*, vol. 20, no. 3, pp. 620–628, 2005.

[5] A. Boglietti, A. Cavagnino, and D. Staton, "Determination of critical parameters in electrical machine thermal models," *IEEE Transactions on Industry Applications*, vol. 44, no. 4, pp. 1150–1159, 2008.

[6] A. Boglietti, E. Carpaneto, M. Cossale, and S. Vaschetto, "Stator-winding thermal models for short-time thermal transients: Definition and validation," *IEEE Transactions on Industrial Electronics*, vol. 63, no. 5, pp. 2713–2721, 2016.

[7] C. Kral, A. Haumer, and T. Bauml, "Thermal model and behavior of a totally-enclosed-water-cooled squirrel-cage induction machine for traction applications," *IEEE Transactions on Industrial Electronics*, vol. 55, no. 10, pp. 3555–3565, 2008.

[8] C. Kral, A. Haumer, and S. B. Lee, "A practical thermal model for the estimation of permanent magnet and stator winding temperatures," *IEEE Transactions on Power Electronics*, vol. 29, no. 1, pp. 455–464, 2014.

[9] S. Nategh, O. Wallmark, M. Leksell, and S. Zhao, "Thermal analysis of a pmasrm using partial fea and lumped parameter modeling," *IEEE Transactions on Energy Conversion*, vol. 27, no. 2, pp. 477–488, 2012.

[10] C. Sciascera, P. Giangrande, L. Papini, C. Gerada, and M. Galea, "Analytical thermal model for fast stator winding temperature prediction," *IEEE Transactions on Industrial Electronics*, vol. 64, no. 8, pp. 6116–6126, 2017.

[11] J. P. C. Smeets, J. Soulard, and E. A. Lomonova, "Thermal analysis of a winding turn-to-turn fault in PM synchronous machine," in *The XIX International Conference on Electrical Machines - ICEM 2010*. IEEE, sep 2010.

[12] L. Chen, J. Wang, and Z. Sun, "Electromagnetic-thermal coupled modelling and analysis of inter-turn short-circuit faults of a permanent magnet alternator," *The Journal of Engineering*, vol. 2019, no. 17, pp. 4426–4431, jun 2019.

[13] B. Jux and M. Doppelbauer, "Impact of inter-turn fault onto the transient thermal machine behaviour and fault development," in *The 10th International Conference on Power Electronics, Machines and Drives(PEMD)*. IEEE, dec 2020.

[14] F. Hoffmann, B. Jux, and M. Doppelbauer, "Thermal modeling of the stator slot in electrical machines using an extended layer approach," in *IECON 2019 - 45th Annual Conference of the IEEE Industrial Electronics Society*. IEEE, oct 2019.

[15] S. Foitzik and M. Doppelbauer, "Simulation of stator winding faults with an analytical model of a PMSM," in *2018 IEEE International Conference on Power Electronics, Drives and Energy Systems (PEDES)*. IEEE, dec 2018.

[16] B.-G. Gu, "Study of IPMSM interturn faults part II: Online fault parameter estimation," *IEEE Transactions on Power Electronics*, vol. 31, no. 10, pp. 7214–7223, oct 2016.

[17] S. Foitzik and M. Doppelbauer, "Fault tolerant control of 3ph pmsm with inter-turn faults," in *The 10th International Conference on Power Electronics, Machines and Drives (PEMD)*. IEEE, dec 2020.

[18] F. Hoffmann and M. Doppelbauer, "Extended layer approach for thermal modeling of a tooth-coil winding in electrical machines," in *The 10th International Conference on Power Electronics, Machines and Drives (PEMD)*. IEEE, dec 2020.